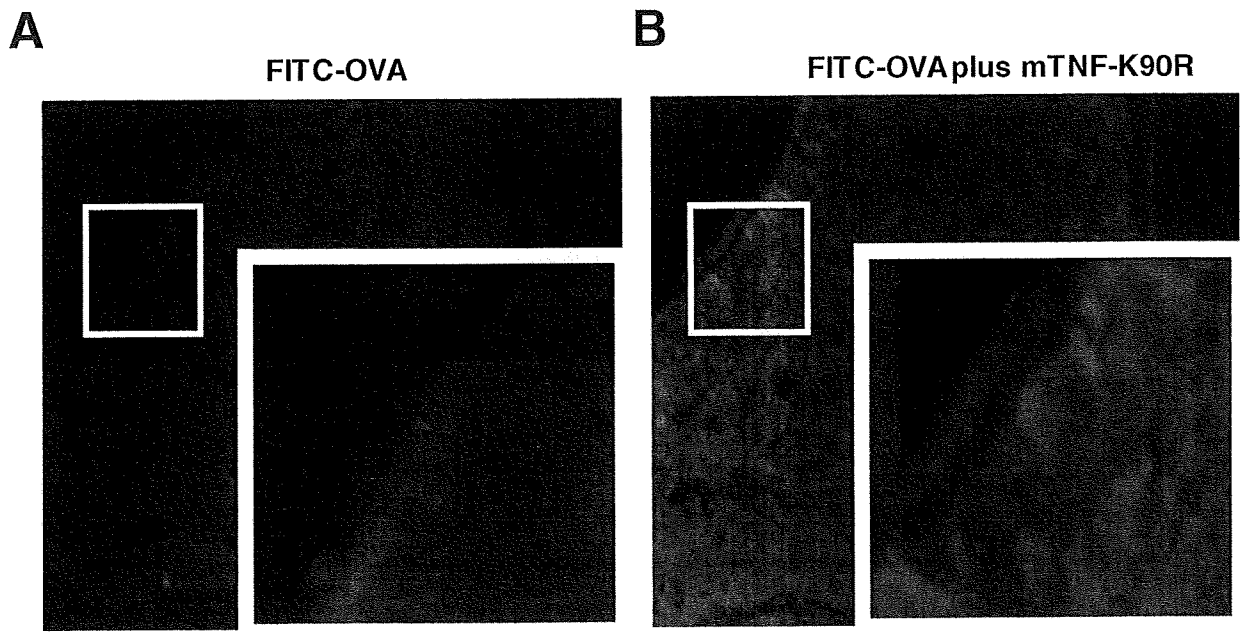

Figure 8. Localization analysis of OVA in NALT. BALB/c mice were administered 50 μg FITC-OVA and a combination of 5 μg mTNF-K90R as a nasal vaccine adjuvant. Frozen sections of NALT resected from mice treated with FITC-OVA alone (A) and a combination of mTNF-K90R (B). The FITC-OVA (green) signals were detected by fluorescence microscopy. The nucleus was counterstained using PI (red). The original magnification of these photographs was 20 ×.

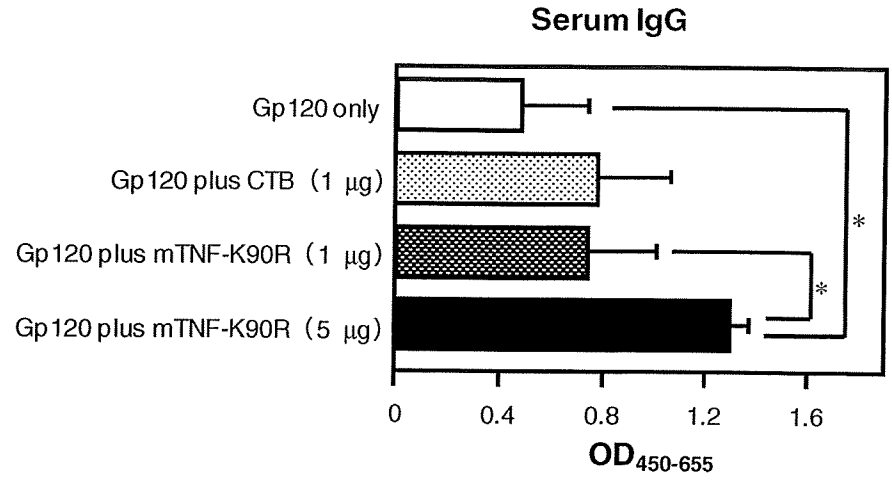

Figure 9. Serum gp120-specific IgG responses following nasal immunization with gp120 plus mTNF-K90R. BALB/c mice were intranasally immunized with gp120 alone, gp120 plus CTB, or gp120 plus mTNF-K90R, four times at weekly intervals. Serum was collected 7 days after the last immunization and analyzed by ELISA for gp120-specific total IgG at a 100-fold serum dilution. Data are presented as mean ± SEM (n = 6; * $P < 0.05$).

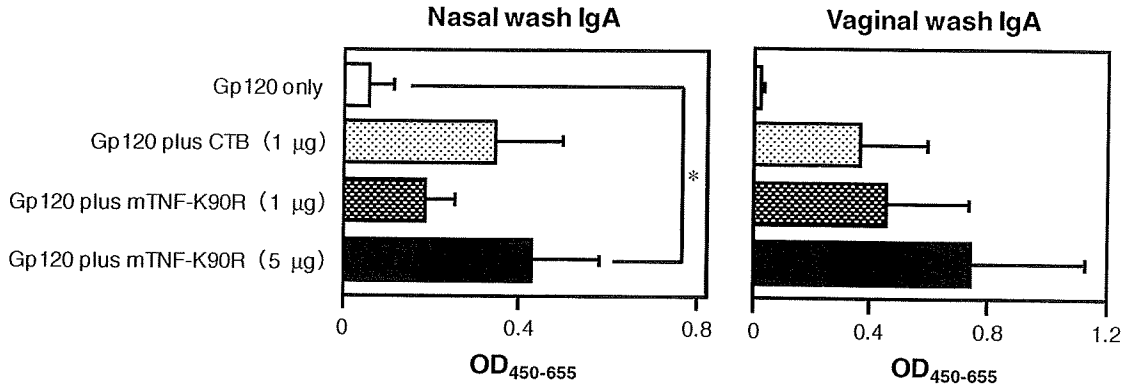

Figure 10. gp120-specific mucosal IgA responses following nasal immunization with gp120 plus mTNF-K90R. BALB/c mice were intranasally immunized with gp120 alone, gp120 plus CTB, or gp120 plus mTNF-K90R once a week for four weeks. Mucosal secretions were collected 7 days after the last immunization and analyzed by ELISA for gp120-specific IgA in 8-fold diluted nasal wash or vaginal wash. Data are presented as mean ± SEM (n = 6; * $P < 0.05$).

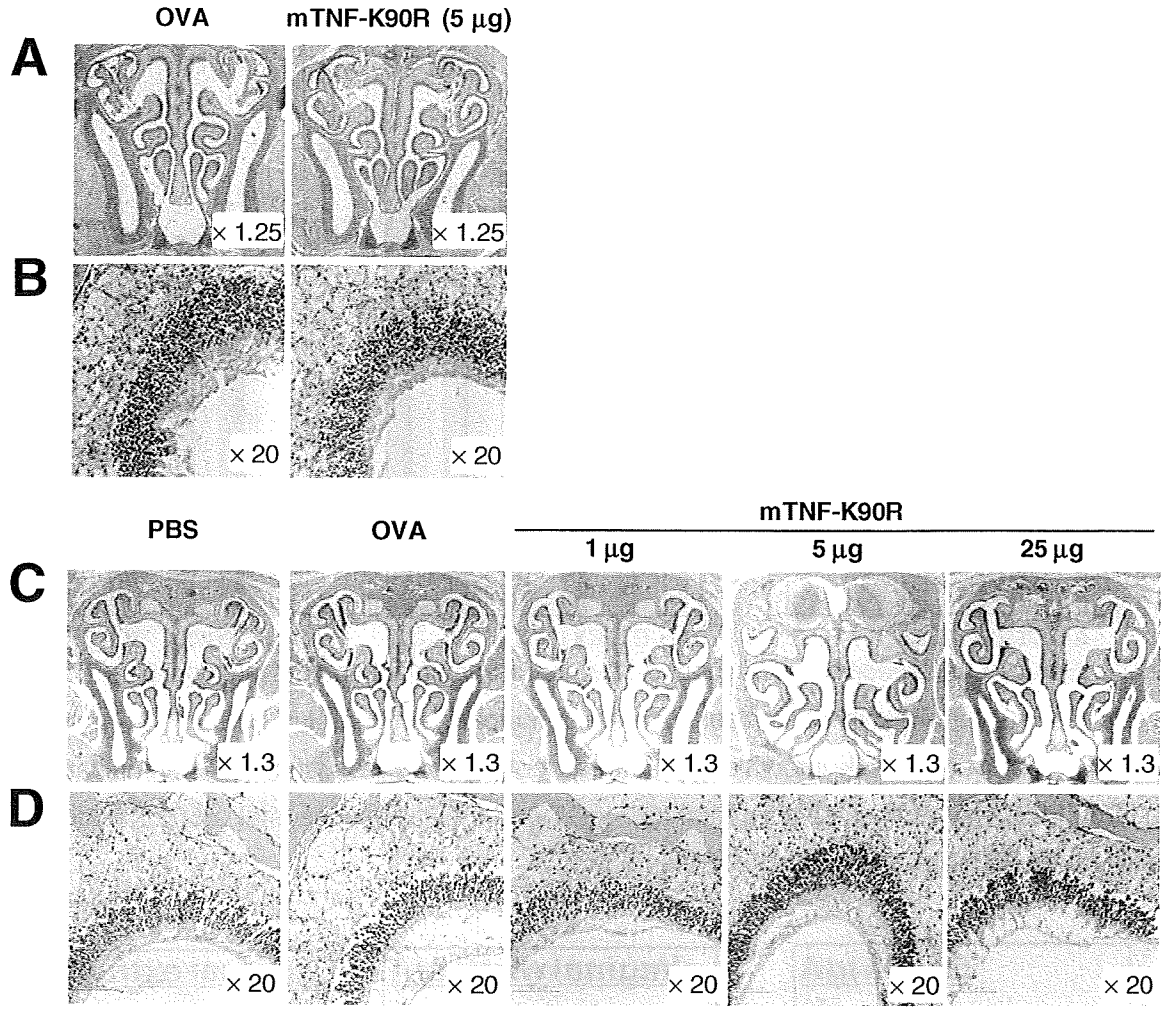

Figure 11. Histopathological analysis of nasal cavity treated with mTNF-K90R. Frontal cross-sections of the nasal cavity from mice, taken 2 h after administration (A, B) or one week after three times administration of PBS, OVA alone, and OVA together with 1 μg, 5 μg or 25 μg mTNF-K90R (C, D). An overall view of the nasal passage is shown in (A) and (C). The region of nasal olfactory epithelia is shown in (B) and (D). Sections were prepared and the tissues were stained with H&E to assess the degree of tissue injury and local inflammation.

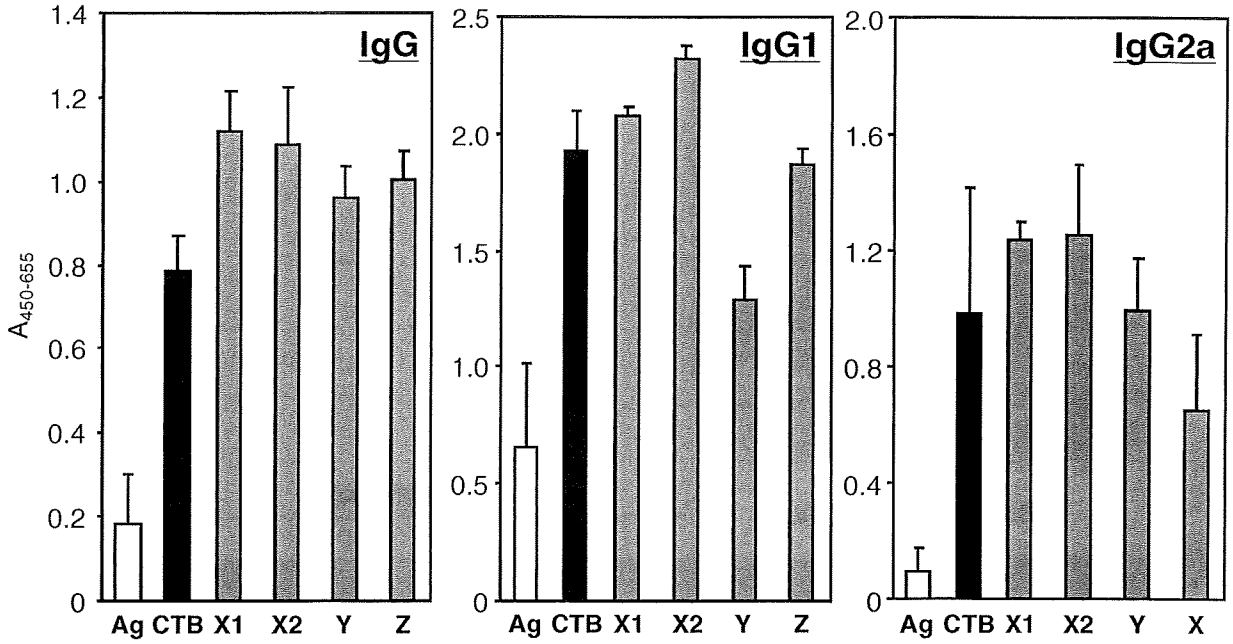

Figure 12. Serum OVA-specific IgG responses by nasal immunization with antigen plus cytokines. BALB/c mice were intranasally immunized with antigen alone, antigen plus CTB, or OVA plus each cytokine two times at 4 week intervals. Serum was collected 7 days after last immunization and analyzed by ELISA for antigen-specific total IgG, IgG1 and IgG2a responses at a 500 fold dilution of serum. Data are presented as means ± SEM (n = 5).

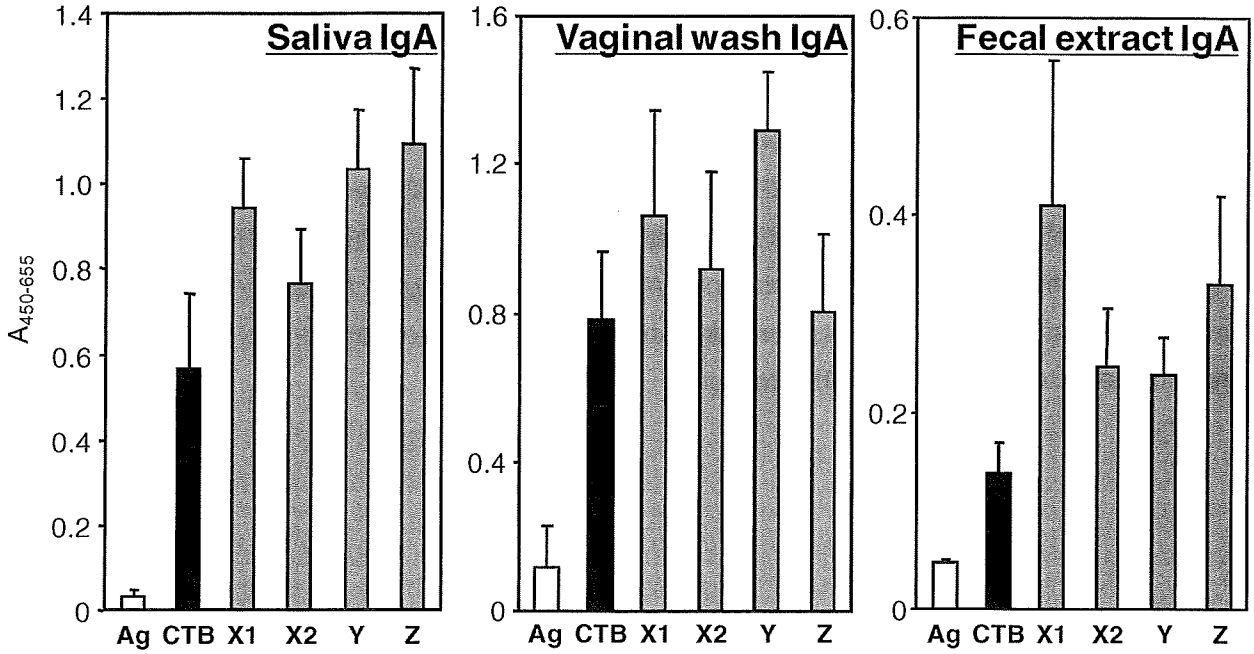

Figure 13. HA-specific mucosal IgA responses by nasal immunization with OVA plus cytokines. BALB/c mice were intranasally immunized with HA alone, HA plus CTB, or OVA plus each cytokine two times at 4 week intervals. Mucosal secretions was collected seven days after last immunization and OVA-specific IgA responses in (A) saliva, (B) vaginal wash and (C) fecal extract were determined by ELISA, respectively. Data are presented as means ± SEM (n = 5).

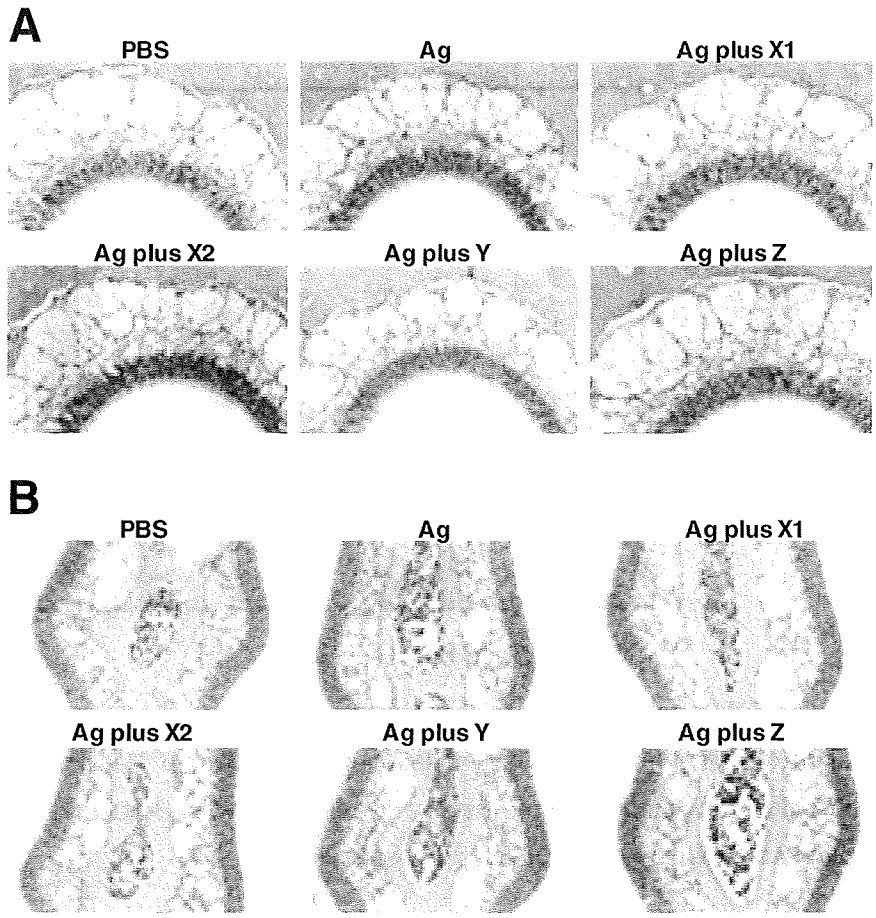

Figure 14. Histopathological analysis of the nasal cavity treated with cytokine. Frontal cross-sections of the nasal cavity from mice taken after two administrations of PBS, Ag alone or Ag together with cytokine. Sections were prepared and the tissues were stained with H&E (A) or Luna staining (B) to assess the degree of pathological changes. An overall view of the nasal epithelium (A) and Luna-stained eosinophils in the nasal septum (B) are shown, respectively.

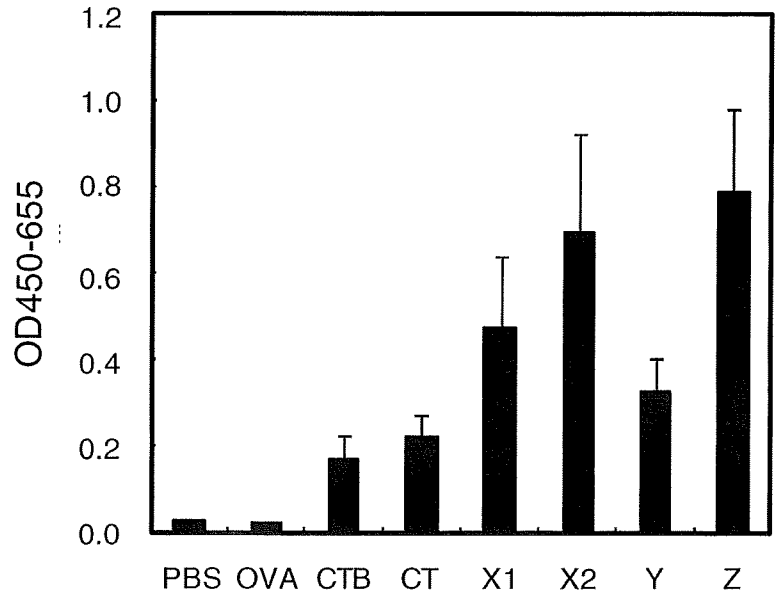

Figure 15. Serum OVA-specific IgE responses following nasal immunization with OVA plus each indicated cytokine. BALB/c mice were intranasally immunized with OVA alone, OVA plus CTB, OVA plus CT, or OVA plus each cytokine three times at weekly intervals. Serum was collected 7 days after last immunization and analyzed by ELISA for OVA-specific IgE.

研究成果の刊行に関する一覧表

雑誌

発表者氏名	論文タイトル名	発表誌名	巻号	ページ	出版年
Shibata H, Kamada H, Kobayashi-Nishibata K, Yoshioka Y, Nishibata T, Abe Y, Nomura T, Nabeshi H, Minowa K, Mukai Y, Nakagawa S, Mayumi T, Tsunoda S, Tsutsumi Y.	Role of amino acid residue 90 in bioactivity and receptor binding capacity of tumor necrosis factor mutants.	Biochim Biophys Acta	1774(8)	1029-35	2007
Shibata H, Yoshioka Y, Ohkawa A, Minowa K, Mukai Y, Abe Y, Taniai M, Nomura T, Kayamuro H, Nabeshi H, Sugita T, Imai S, Nagano K, Yoshikawa T, Fujita T, Nakagawa S, Yamamoto A, Ohta T, Hayakawa T, Mayumi T, Vandenabeele P, Aggarwal BB, Nakamura T, Yamagata Y, Tsunoda S, Kamada H, Tsutsumi Y.	Creation and X-ray structure analysis of the tumor necrosis factor receptor-1-selective mutant of a tumor necrosis factor-alpha antagonist.	J Biol Chem	283(2)	998-1007	2008
Imai S, Mukai Y, Takeda T, Abe Y, Nagano K, Kamada H, Nakagawa S, Tsunoda S, Tsutsumi Y.	The effect of protein properties on display efficiency using the M13 phage display system.	Pharmazie	63(10)	760-764	2008
Abe Y, Yoshikawa T, Kamada H, Shibata H, Nomura T, Minowa K, Kayamuro H, Katayama K, Miyoshi H, Mukai Y, Yoshioka Y, Nakagawa S, Tsunoda S, Tsutsumi Y.	Simple and highly sensitive assay system for TNFR2-mediated soluble- and transmembrane-TNF activity.	J. Immunol. Methods	335(1-2)	71-8	2008

Kayamuro H, Abe Y, Yoshioka Y, Katayama K, Nomura T, Yoshida T, Yamashita K, Yoshikawa T, Kawai Y, Mayumi T, Hiroi T, Itoh N, Nagano K, Kamada H, Tsunoda S, Tsutsumi Y.	The use of a mutant TNF-α as a vaccine adjuvant for the induction of mucosal immune responses.	Biomaterials	30(29)	5869-76	2009
Kayamuro H, Yoshioka Y, Abe Y, Katayama K, Yoshida T, Yamashita K, Yoshikawa T, Hiroi T, Itoh N, Kawai Y, Mayumi T, Kamada H, Tsunoda S, Tsutsumi Y.	TNF superfamily member, TL1A, is a potential mucosal vaccine adjuvant.	Biochem Biophys Res Commun	384(3)	296-300	2009
Kayamuro H, Abe Y, Yoshioka Y, Katayama K, Yoshida T, Yamashita K, Yoshikawa T, Kawai Y, Mayumi T, Hiroi T, Ito N, Nagano K, Kamada H, Tsunoda S, Tsutsumi Y.	Mutant TNF-α, mTNF-K90R, is a novel mucosal vaccine adjuvant candidate against HIV.	Pharmazie			In press

THE JOURNAL OF BIOLOGICAL CHEMISTRY VOL. 283, NO. 2, pp. 998–1007, January 11, 2008
© 2008 by The American Society for Biochemistry and Molecular Biology, Inc. Printed in the U.S.A.

Creation and X-ray Structure Analysis of the Tumor Necrosis Factor Receptor-1-selective Mutant of a Tumor Necrosis Factor-α Antagonist*

Received for publication, September 21, 2007, and in revised form, November 2, 2007 Published, JBC Papers in Press, November 14, 2007, DOI 10.1074/jbc.M707933200

Hiroko Shibata,[a,b] Yasuo Yoshioka,[a,c] Akiko Ohkawa,[a] Kyoko Minowa,[a,d] Yohei Mukai,[a,e] Yasuhiro Abe,[a,e] Madoka Taniai,[f] Tetsuya Nomura,[a,e] Hiroyuki Kayamuro,[a,e] Hiromi Nabeshi,[a,e] Toshiki Sugita,[a,e] Sunao Imai,[a,e] Kazuya Nagano,[a,e] Tomoaki Yoshikawa,[a] Takuya Fujita,[d] Shinsaku Nakagawa,[c,e] Akira Yamamoto,[d] Tsunetaka Ohta,[f] Takao Hayakawa,[b] Tadanori Mayumi,[g] Peter Vandenabeele,[h] Bharat B. Aggarwal,[i] Teruya Nakamura,[j] Yuriko Yamagata,[j] Shin-ichi Tsunoda,[a,c] Haruhiko Kamada,[a,c1] and Yasuo Tsutsumi[a,c,e]

From the [a]National Institute of Biomedical Innovation, 7-6-8 Saito-Asagi, Ibaraki, Osaka 567-0085, Japan, [b]National Institute of Health Science, 1-18-1 Kamiyoga, Setagaya-ku, Tokyo 158-8501, Japan, [c]Center for Advanced Medical Engineering and Informatics, Osaka University, 1-6 Yamadaoka, Suita, Osaka 565-0871, Japan, [d]Kyoto Pharmaceutical University, Misasagi-Nakauchicho 5, Yamashina-ku, Kyoto 607-8414, Japan, [e]Graduate School of Pharmaceutical Sciences, Osaka University, 1-6 Yamadaoka, Suita, Osaka 565-0871, Japan, [f]Hayashibara Biochemical Laboratories, Inc., 1-2-3 Shimoishii, Okayama 702-8006, Japan, [g]Graduate School of Pharmaceutical Sciences, Kobe Gakuin University, 518 Arise, Igawadani, Nishi-ku, Kobe 651-2180, Japan, the [h]Department of Molecular Biomedical Research, Flanders Institute for Biotechnology and the Department of Molecular Biology, Ghent University, B-9052 Ghent, Belgium, the [i]Department of Experimental Therapeutics, University of Texas M. D. Anderson Cancer Center, Houston, Texas 77030, and [j]Faculty of Medical and Pharmaceutical Sciences, Kumamoto University, 5-1 Ooehonmachi, Kumamoto 862-0973, Japan

Tumor necrosis factor-α (TNF) induces inflammatory response predominantly through the TNF receptor-1 (TNFR1). Thus, blocking the binding of TNF to TNFR1 is an important strategy for the treatment of many inflammatory diseases, such as hepatitis and rheumatoid arthritis. In this study, we identified a TNFR1-selective antagonistic mutant TNF from a phage library displaying structural human TNF variants in which each one of the six amino acid residues at the receptor-binding site (amino acids at positions 84–89) was replaced with other amino acids. Consequently, a TNFR1-selective antagonistic mutant TNF (R1antTNF), containing mutations A84S, V85T, S86T, Y87H, Q88N, and T89Q, was isolated from the library. The R1antTNF did not activate TNFR1-mediated responses, although its affinity for the TNFR1 was almost similar to that of the human wild-type TNF (wtTNF). Additionally, the R1antTNF neutralized the TNFR1-mediated bioactivity of wtTNF without influencing its TNFR2-mediated bioactivity and inhibited hepatic injury in an experimental hepatitis model. To understand the mechanism underlying the antagonistic activity of R1antTNF, we analyzed this mutant using the surface plasmon resonance spectroscopy and x-ray crystallography. Kinetic association/dissociation parameters of the R1antTNF were higher than those of the wtTNF, indicating very fast bond dissociation. Furthermore, x-ray crystallographic analysis of R1antTNF suggested that the mutation Y87H changed the binding mode from the hydrophobic to the electrostatic interaction, which may be one of the reasons why R1antTNF behaved as an antagonist. Our studies demonstrate the feasibility of generating TNF receptor subtype-specific antagonist by extensive substitution of amino acids of the wild-type ligand protein.

Tumor necrosis factor (TNF)[2] is a major inflammatory cytokine that, like the other members of the TNF superfamily of ligands, plays a central role in host defense and inflammation (1). Elevated serum levels of TNF correlate with the severity and progression of the inflammatory diseases such as rheumatoid arthritis, inflammatory bowel disease, septic shock, multiple sclerosis, and hepatitis (2–4). So far, anti-TNF antibodies and soluble TNFRs, which interfere with the activity of TNF, have been used to treat various inflammatory diseases (5, 6). However, these therapies can cause serious side effects, such as bacterial and virus infection, lymphoma development, and lupus inflammatory disease (7–10), because they also inhibit the TNF-

* This work was supported in part by Grants-in-aid for Scientific Research 18015055, 18659047, and 7689008 from the Ministry of Education, Culture, Sports, Science and Technology of Japan and Japan Society for the Promotion of Science, by a Health Labor Sciences research grant from the Ministry of Health, Labor and Welfare of Japan, by Health Sciences research grants for research on health sciences focusing on drug innovation from the Japan Health Sciences Foundation, and in part by Japan Society for the Promotion of Science Research Fellowships for Young Scientists 02872, 08841, 09131. The costs of publication of this article were defrayed in part by the payment of page charges. This article must therefore be hereby marked "*advertisement*" in accordance with 18 U.S.C. Section 1734 solely to indicate this fact.

The atomic coordinates and structure factors (code 2E7A) have been deposited in the Protein Data Bank, Research Collaboratory for Structural Bioinformatics, Rutgers University, New Brunswick, NJ (http://www.rcsb.org/).

[1] To whom correspondence should be addressed: Laboratory of Pharmaceutical Proteomics, National Institute of Biomedical Innovation, 7-6-8 Saito-Asagi, Ibaraki, Osaka 567-0085, Japan. Fax: 81-72-641-9817; E-mail: kamada@nibio.go.jp.

[2] The abbreviations used are: TNF, tumor necrosis factor α; TNFR, TNF receptor; PDB, Protein Data Bank; PBS, phosphate-buffered saline; RT, reverse transcription; HUVEC, human umbilical vein endothelial cells; ELISA, enzyme-linked immunosorbent assay; GM-CSF, granulocyte-macrophage colony-stimulating factor; TES, 2-{[2-hydroxy-1,1-bis(hydroxymethyl)ethyl]amino}ethanesulfonic acid; EAE, experimental autoimmune encephalomyelitis; ALT, alanine aminotransferase; h, human; m, mouse; mut, mutant.

The Journal of Biological Chemistry

Downloaded from www.jbc.org at OSAKA UNIVERSITY on March 13, 2008

dependent host defense function of the patients. TNF blockade by administering these agents into patients with multiple sclerosis was also shown to aggravate their symptoms (11). Therefore, to overcome these problems, development of a new therapeutic strategy is highly desirable.

TNF binds to two receptor subtypes, p55 TNF receptor (TNFR1) and p75 TNF receptor (TNFR2), to exert its biological functions (12). Thus, functional analyses of the TNF receptors were carried out to explore a new therapeutic strategy. Previous studies using animal models of diseases such as arthritis and hepatitis demonstrated the predominant role of TNFR1 in the pathogenesis and exacerbation of inflammation (13, 14). In the experimental autoimmune encephalomyelitis model (EAE), which is widely used as an animal model of multiple sclerosis, the symptoms exacerbated significantly in the TNF knock-out mice compared with that in the wild-type mice (15). Another study indicates that the TNF has a dual role on the EAE model, an inflammatory and immunosuppressive effect, and although the immunosuppressive effect does not require the TNFR1, it is essential for the acute phase inflammation of EAE (16). On the other hand, although the TNFR1 is believed to be important for the defense mechanism against mycobacterium, the membrane-bound TNF, the prime activating ligand of TNFR2, was reported to be sufficient to control the mycobacterial infection (17, 18). Moreover, TNFR2 was shown to be crucial for the proliferation, activation, and antigen presentation of the T-cells, which are essential in the cell-mediated immune response against bacteria and virus (19–21). Therefore, blocking the TNFR1-mediated signal transduction emerged as a potential therapeutic strategy with low side effects for the inflammatory diseases.

From these perspectives, attempts were made to develop drugs targeted to TNFR1. Along with the progress of antibody engineering, attempts were made to develop an anti-TNFR1 antibody with antagonistic activity. But the desired antibody could not be created, because the anti-TNFR1 antibodies recognizing the TNF-binding site on TNFR1 acted like a TNFR1 agonist and not an antagonist (22). Attempts to design a low molecular weight TNFR1 antagonist based on the three-dimensional structural information of the TNFR1 was also not successful in identifying an antagonist that would selectively inhibit the TNF/TNFR1 interaction and would have sufficient therapeutic effect (23, 24). In this respect, we previously 1) constructed two phage libraries displaying the structural TNF variants in which six amino acid residues (amino acids 29, 31, 32, 145–147, library I; amino acids 84–89, library II) in the predicted receptor binding sites were replaced with other amino acid, 2) and we successfully identified the TNFR1-selective mutant with great biological activity from the library I.[3] In the screening process, mutants with high affinity for the TNFR1 and great TNFR1 selectivity were found from library II, although their biological activities were very weak.[3] The strategy described here could comprehensively assess the affinities and bioactivities of TNF variants, thus enabling the high-throughput screening of TNFR1-selective antagonists, which have no biological activity but high TNFR1 affinity. In this study, we analyzed the biological activity and TNFR1 affinity of 500 TNF variants, which were concentrated by panning against the TNFR1, and we subsequently isolated a novel TNFR1-selective antagonistic mutant TNF (R1antTNF). R1antTNF showed exclusive TNFR1 selectivity, and it efficiently inhibited wide varieties of TNFR1-mediated effects of the wild-type TNF *in vitro* and *in vivo*. Additionally, we used surface plasmon resonance and x-ray structural analyses to elucidate the underlying cause for the antagonist activity of R1antTNF.

[3] Y. Abe, H. Shibata, K. T. Nomura, K. Minowa, H. Kamada, S. Tsunoda, Y. Tsutsumi, unpublished data.

EXPERIMENTAL PROCEDURES

Cell Culture—L-M cells (a mouse fibroblast cell line) were provided by Mochida Pharmaceutical Co. Ltd. (Tokyo, Japan) and were maintained in minimum Eagle's medium (Sigma) supplemented with 1% fetal bovine serum and 1% antibiotic mixture (penicillin 10,000 units/ml, streptomycin 10 mg/ml, and amphotericin B 25 μg/ml) (Nacalai Tesque, Kyoto, Japan). HEp-2 cells (a human fibroblast cell line) were provided by Cell Resource Center for Biomedical Research (Tohoku University, Sendai, Japan) and were maintained in RPMI 1640 medium (Sigma) supplemented with 10% fetal bovine serum and 1% antibiotic mixture (Nacalai Tesque). PC60-R1 and PC60-R2 cells (a mouse-rat fusion hybridoma consisting of human TNFR1- or TNFR2-transfected PC60 cells) were established as described previously (25) and maintained in RPMI 1640 medium supplemented with 10% fetal bovine serum, 1 mM sodium pyruvate, 5×10^{-5} M 2-mercaptoethanol, 3 μg/ml puromycin (Wako Pure Chemical Industries, Osaka, Japan), and 1% antibiotic mixture.

Cytokines, Receptors, and Antibodies—Recombinant human TNFR1 or TNFR2 Fc chimera, biotinylated anti-human TNF polyclonal antibody, and horseradish peroxidase-conjugated horseradish peroxidase were purchased from R & D Systems (Minneapolis, MN). Recombinant human or mouse TNF and IL-1β were purchased from PeproTech (Rocky Hill, NJ). The recombinant human TNF used for the *in vivo* hepatitis examination and the recombinant wtTNF-FLAG (a FLAG tag fusion protein of human TNF) were purified in our laboratory. We confirmed that the bioactivity of each TNF was equal to that of commercially available recombinant human TNF. Anti-FLAG M2 antibody was purchased from Sigma. Goat anti-human IgG antibody was purchased from Cappel (West Chester, PA). Anti-human Fas IgM was purchased from MBL (Nagoya, Japan).

Selection of Phage Displaying Structural TNF Variants (Panning)—Human TNFR1 Fc chimera was diluted to 50 μg/ml in 10 mM sodium acetate buffer, pH 4.5, and immobilized to a CM3 sensor chip using an amine coupling kit (BIAcore®, Uppsala, Sweden), which resulted in an increase of 4,000–6,000 resonance units. The phage library (1×10^{11} colony-forming units/100 μl) was injected at the flow rate of 3 μl/min over the sensor chip. After injection, the sensor chip was washed using the rinse command. Elution was carried out using 20 μl of 10 mM glycine HCl. The eluted phages were neutralized with 1 M Tris-HCl, pH 6.9. *Escherichia coli* (TG1) was infected with the eluted phages for amplification. These steps were performed twice. After the second round of selection, the phage mixture was used to infect *E. coli* and plated on LB agar/ampicillin

Downloaded from www.jbc.org at OSAKA UNIVERSITY on March 13, 2008

plates. Five hundred individual colonies of *E. coli* infected with phage clones were individually picked from the LB agar plates, and each colony was grown in 2-YT medium with ampicillin (100 μg/ml) and glucose (2% w/v) at 37 °C until the A_{600} of the culture medium reached 0.4. Each culture was centrifuged; the supernatants were removed, and fresh 2-YT media with ampicillin (100 μg/ml) was added to each *E. coli* pellet. After incubation for 6 h at 37 °C, supernatants were collected and used to measure cytotoxicity in human HEp-2 cells (26, 27) and to determine the affinity for TNFR1 by ELISA (28). To measure cytotoxicity, HEp-2 cells were cultured in 96-well plates with 10% *E. coli* supernatant and 100 μg/ml cycloheximide for 18 h at 4×10^4 cells/well, and cytotoxicity was assessed by methylene blue assay as described previously (26). To determine the affinity for TNFR1 by ELISA, wells of the immune assay plates were first coated with the goat anti-human IgG antibody and then incubated with the recombinant human TNFR1 Fc chimera (0.2 μg/ml). After blocking, 2-fold diluted *E. coli* supernatant was added into each well, and the plates were incubated for 2 h at 37 °C. To each well, 200 ng/ml biotinylated anti-human TNF polyclonal antibody was added, and the plates were further incubated for 1 h at 37 °C. Wells were washed and then incubated with 1000-fold diluted avidin-horseradish peroxidase. Next, wells were washed; TMB peroxidase substrate (MOSS, Inc. Pasadena, MD) was added to each well, and the absorbance was read at 450/650 nm using a micro-plate reader.

Expression and Purification of mutTNFs—Protocol for the expression and purification of recombinant proteins was described previously (29). Briefly, mutTNFs were overexpressed in *E. coli* BL21(DE3). Expressed mutTNFs were recovered from the inclusion body, which were washed with 2.5% Triton X-100 and 0.5 M NaCl in TES buffer, and solubilized in 6 M guanidine HCl, 0.1 M Tris-HCl, pH 8.0, and 2 mM EDTA. The solubilized protein was reduced with 10 mg/ml dithioerythritol for 4 h at room temperature and then refolded by 100-fold dilution in a refolding buffer (100 mM Tris-HCl, 2 mM EDTA, 0.5 M arginine, and oxidized glutathione (551 mg/liter)). After dialyzing against 20 mM Tris-HCl, pH 7.4, containing 100 mM urea, the active trimeric proteins were purified by Q-Sepharose and Mono Q chromatography. An additional size-exclusion chromatography (Superose 12, GE Healthcare) was performed to further purify each protein. Endotoxin levels in the purified mutTNF were determined to be <300 pg/mg.

Cytotoxicity Assay—For the cytotoxicity assay, mouse L-M cells were cultured in the 96-well plates (1×10^4 cells/well) in the presence of serially diluted mouse wtTNF or mutTNFs. For the neutralization assay, cells were cultured in the presence of a constant concentration of the mouse wtTNF (5 ng/ml) and a serial dilution of the mutTNF. After incubation for 48 h, cell survival was determined by methylene blue assay as described previously (26). Jurkat cells were incubated in 96-well plates (1×10^4 cells/well) with 0.2 ng/ml anti-human Fas IgM and serially diluted R1antTNF for 24 h, and cytotoxicity was assessed using the 3-(4,5-dimethylthiazol-2-yl)-2,5-diphenyltetrazolium bromide assay.

Competitive ELISA—Inhibition of wtTNF binding to the hTNFR1 and hTNFR2 by R1antTNF was measured by ELISA as reported previously (28). The wtTNF-FLAG, a FLAG tag fusion protein of human TNF, was used as a marker protein. Briefly, the immune assay plates were coated with the goat anti-human IgG antibody and incubated with either the human TNFR1 or the human TNFR2 (0.2 μg/ml). After blocking, premixed wtTNF-FLAG (100 ng/ml) and various concentrations of R1antTNF were added to the plates. After 2 h of incubation at room temperature, the wells were washed, and the biotinylated anti-FLAG M2 antibody (0.5 μg/ml) was added to each well and then incubated for an additional period of 2 h at room temperature. Wells were washed and then incubated with the horseradish peroxidase-coupled streptavidin for 30 min at room temperature. The remaining bound wtTNF-FLAG was quantified as described above.

PC60 Assay—PC60-R1 and PC60-R2 cells were cultured at 5×10^4 cells/well with IL-1β (2 ng/ml). To evaluate the inhibitory activity, serially diluted R1antTNF and human wtTNF (200 ng/ml for PC60-R1 and 40 ng/ml for PC60-R2) were added to each cell type. After 24 h of incubation, the amount of rat GM-CSF produced was quantified by ELISA according to the manufacturer's protocol (R & D Systems).

Caspase-3/7 and NF-κB Activities—To measure the caspase-3/7 activity, the L-M cells were incubated with the human wtTNF (60 ng/ml) and R1antTNF for 8 h, and then an equal volume of the Caspase-Glo 3/7 Assay reagent (Promega Japan, Tokyo, Japan) was added to the cells. The cells were further incubated for 1 h, and luminescence was then measured using a plate reader (ALVO series, PerkinElmer Life Sciences). To measure the NF-κB activity, nuclear proteins were collected from the L-M cells stimulated with the human wtTNF (5 ng/ml) and R1antTNF for 1 h, and the activity of the NF-κB p65 in the treated cells was determined using the TransAM NF-κB p65 kit (Active Motif, Carlsbad, CA). Nuclear protein extract (1 μg) was added to an oligonucleotide-coated plate and was visualized using an anti-NF-κB p65 antibody.

RT-PCR Analysis—Total RNA was extracted from the human wtTNF and R1antTNF-stimulated HUVEC using an RNeasy mini kit (Qiagen, Valencia, CA). First-strand cDNA was synthesized from 1 μg of total RNA by using an oligo(dT_{12-18}) primer and SuperScript III reverse transcriptase (Invitrogen). Real time quantitative RT-PCR was performed using the TaqMan assay, and the PCR amplifications were carried out using an ABI 7000 thermocycler (Applied Biosystems, Foster City, CA). cDNA samples were added into a PCR master mix containing the Platinum qPCR super mix (Invitrogen) and primer/fluorescent probe sets (TaqMan Gene Expression Assays, Applied Biosystems) for the human β-actin, E-selectin, and ICAM-1 in 96-well PCR plates. Conditions for PCR were 2 min at 50 °C, 2 min at 95 °C, 45 cycles of denaturation at 95 °C for 15 s, and annealing/extension step at 60 °C for 5 s. The threshold cycle (*CT*) during the exponential phase of amplification was determined using the ABI Prism® 7000 SDS software.

Induction of Lethal Hepatitis—BALB/c mice (6-week-old females) were purchased from CLEA Japan (Tokyo, Japan). All experimental protocols for animal studies were in accordance with "Principles of Laboratory Animal Care" (National Institutes of Health) and our institutional guidelines. All reagents were prepared in pyrogen-free PBS. Control mice were injected

Downloaded from www.jbc.org at OSAKA UNIVERSITY on March 13, 2008

intravenously with 200 μl of the mixture, 100 μl of PBS, 50 μl of 20 μg/ml wtTNF, and 50 μl of 400 mg/ml GalN. Experimental mice were injected intravenously with 200 μl of the mixture, 100 μl of R1antTNF (2.7, 0.3, or 0.1 mg/ml), 50 μl of 20 μg/ml wtTNF, and 50 μl of 400 mg/ml GalN. In preliminary experiments, serum ALT levels began to increase at 6 h and were maximal 9 h after the administration of TNF/GalN. The dose used was lethal in 80–100% of mice. Blood samples were obtained from the orbital plexus under light ether anesthesia 9 h after the challenge. The serum ALT concentration was measured using a colorimetric assay kit from Wako Pure Chemical (Osaka, Japan).

Surface Plasmon Resonance Assay (BIAcore® Assay)—The binding kinetics of the wtTNF and R1antTNF were analyzed by the surface plasmon resonance (BIAcore®) technique. TNFRs were immobilized onto a CM5 sensor chip, which resulted in an increase of 3,000–3,500 resonance units. During the association phase, R1antTNF or wtTNF, diluted in running buffer (HBS-EP) at 26.1 nM, 8.7 nM or 2.9 nM, was allowed to pass over the immobilized TNFRs at a flow rate of 20 μl/min. During the dissociation phase, HBS-EP buffer was applied to the sensor chip at a flow rate of 20 μl/min. The data were analyzed globally with the BIAevaluation 3.0 software (BIAcore®) using a 1:1 binding model.

X-ray Crystallography—Purified R1antTNF was concentrated to 10 mg/ml in 20 mM Tris-HCl, pH 7.4. Initial screening using Hampton Crystal screen 1, 2 and Index kit was performed by the vapor-diffusion method with hanging drops (1 + 1 μl) at 20 °C. After optimization of crystallization conditions, orthorhombic crystals ($0.2 \times 0.2 \times 0.4$ mm^3) were obtained with 0.05 M HEPES, pH 7.5, 1.5% w/v 1,2,3-heptanetriol, and 12.5% PEG 3350. Crystals were frozen in a reservoir solution containing 20% glycerol as a cryoprotectant. X-ray diffraction data to 1.8 Å resolution were collected at the BL41XU, SPring-8 synchrotron, Harima, Japan, under flash-cooling to 100 K to reduce the effects of radiation damage. Data reduction was carried out using the DENZO and SCALEPACK. Molecular replacement was performed by using the Molrep program in ccp4i (30) using a crystal structure of the wtTNF (1TNF) (31) as a model. Cycles of manual rebuilding using O (32) and refinement using CNS (33) led to a refined structure. Final model validation was performed using the Procheck program in ccp4i (30). The model complexes of TNF-TNFR1 and R1antTNF-TNFR1 were constructed based on the crystal structure of the LT-α-TNFR1 complex (31) by using the superpose program in ccp4i.

RESULTS

Selection of TNFR1-selective mutTNF Antagonists—We previously constructed a phage library that displays structural variants of the human TNF in which random amino acid sequences replace the 6 residues (amino acids 84–89) that have been predicted to be in the TNF receptor-binding site from the crystal structure of the LT-α-TNFR1 complex (31). We confirmed that the phage library consisted of 1×10^7 independent recombinant clones. To isolate a TNFR1-selective mutant TNF (mutTNF) antagonist, the phage library was subjected to two rounds of panning against the human TNFR1 (hTNFR1) using the BIAcore® biosensor, and recovered clones were assessed for

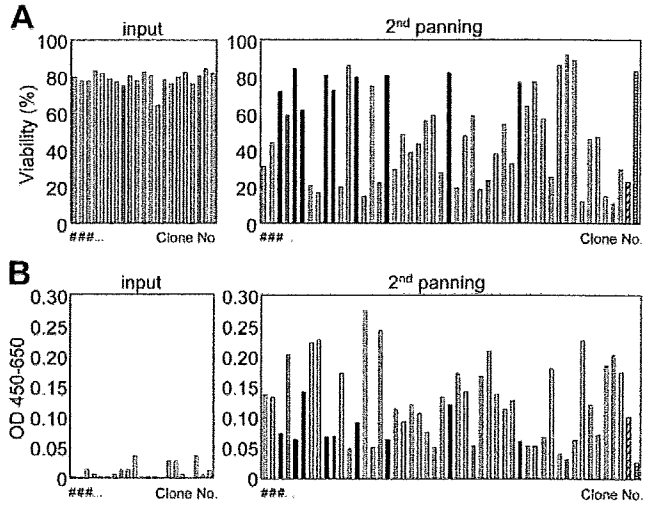

FIGURE 1. **Screening of TNFR-selective mutTNFs with no bioactivity.** Selected phage clones from the phage library were used to infect *E. coli* in a 96-well plate, and the supernatant from each infected *E. coli* was assessed to determine the bioactivity (*A*) and binding affinity (*B*) of each mutTNF. *A*, Hep-2 cells were incubated with the *E. coli* supernatant for 18 h, and cell viability was measured using the methylene blue assay. *B*, each *E. coli* supernatant was applied to the TNFR1-immobilized plate, and binding of the mutTNF to the TNFR1 was detected using the biotinylated polyclonal anti-TNF antibody. ■, mutTNF clones binding specifically to TNFR1; ▨, wtTNF; ▤, negative control.

TABLE 1
Nucleotide and amino acid sequences of 10 candidate TNFR1-selective mutTNF antagonists, which had high affinity for TNFR1 and no TNFR1 bioactivity

Clone	Position					
	Ala-84	Val-85	Ser-86	Tyr-87	Gln-88	Thr-89
T1	G(GGC)	H(CAC)	L(TCC)	Y(TAC)	T(ACG)	T(AAC)
T2	S(AGC)	T(ACC)	T(ACC)	H(CAC)	N(AAC)	Q(CAG)
T3	T(ACC)	S(AGC)	V(GTC)	Y(TAC)	P(CCC)	H(CAC)
T4	T(ACC)	N(AAC)	I(ATC)	Y(TAC)	S(AGC)	N(AAC)
T5	N(AAC)	G(GGC)	A(GCG)	Y(TAC)	E(GAG)	T(ACG)
T6	G(GGC)	G(GGC)	P(CCG)	Y(TAC)	Q(CAG)	R(CGG)
T7	S(AGC)	P(CCG)	R(AGG)	V(GTC)	S(TCC)	G(GGC)
T8	T(ACC)	P(CCC)	A(GCC)	I(ATC)	N(AAC)	R(CGG)
T9	A(GCG)	P(CCC)	G(GGC)	Y(TAC)	S(TCC)	H(CAC)
T10	S(TCC)	P(CCC)	Q(CAG)	Y(TAC)	S(AGC)	V(GTC)

TNFR1-mediated cytotoxicity and affinity for TNFR1. Although the number of phage clones that had strong cytotoxicity increased after the second panning, phage clones having almost no cytotoxicity but significant affinity for TNFR1 were also recognized (Fig. 1). Eventually, we identified 10 mutTNF candidates as the TNFR1-selective antagonists (Table 1), and we further investigated the properties of these 10 potential antagonists. All 10 mutTNFs were recombinantly expressed in *E. coli*, out of which we could only purify nine mutTNFs (T1–T4, T6–T10); for some unknown reason, we were unable to purify the mutTNF-T5. All nine purified mutTNFs displayed a molecular mass of 17 kDa by gel electrophoresis and gel filtration analyses and formed homotrimeric complexes in the same manner as the wtTNF (data not shown). We measured the bioactivities and antagonistic activities of nine mutTNFs on the mouse TNFR1 (mTNFR1) using the L-M cells, a cell line derived from the L929 cells, and the results are shown in Fig. 2. The mutTNF-T2 showed the lowest biological activity even when tested at high concentrations (Fig. 2*A*). Both mutTNF-T2 and mutTNF-T7 inhibited the wtTNF-induced cytotoxicity

Downloaded from www.jbc.org at OSAKA UNIVERSITY on March 1?, 08

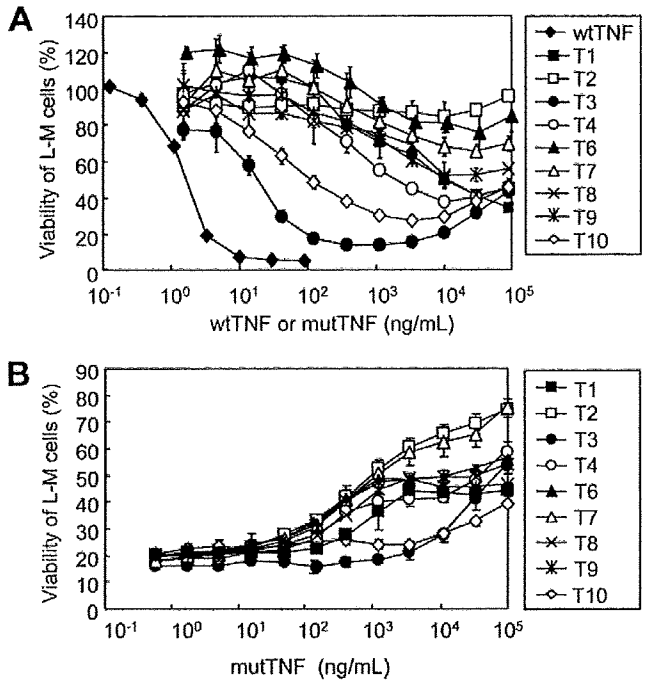

FIGURE 2. **Bioactivities and antagonistic activities of candidate TNFR1-selective mutTNFs.** *A*, diluted mutTNFs were added to the L-M cells and incubated for 48 h at 37 °C. After incubation, cell viability was measured using the methylene blue assay. *B*, indicated dilutions of a given mutTNF and a constant concentration of mouse TNF (5 ng/ml) were mixed and added to the L-M cells. Cell viability was measured as described above, and the antagonistic activity was assessed as described under "Experimental Procedures." Each data point represents the mean ± S.D.

TABLE 2

Dissociation constants of the mutTNFs determined from the SPR analysis of the interactions between the mutTNFs and the hTNFR1 or hTNFR2

Clone	TNFR1 K_D	TNFR2 K_D	TNFR1 selectivity
	nM	*nM*	
wtTNF	1.4	2.1	1.0
T1	5.0	28.1	3.7
T2	3.5	92,900.0	17,677.4
T3	1.2	4.6	2.6
T4	5.0	26.9	3.5
T6	7.6	2.3	0.2
T7	2.3	12.9	3.7
T8	2.6	1230.0	308.8
T9	6.8	8.4	0.8
T10	5.1	8.8	1.1

most efficiently (Fig. 2*B*). Additionally, the TNF receptor selectivity of the nine mutants was measured using the BIAcore® biosensor technique. Both mutTNF-T2 and mutTNF-T8 showed superior TNFR1 selectivity as compared with the other mutants (Table 2). Based on these results, mutTNF-T2 was chosen for further analysis and renamed as R1antTNF; this mutant displayed the highest selectivity for TNFR1 binding and possessed the lowest biological activity and highest antagonistic activity on mTNFR1.

Inhibition of TNFR1-mediated Intracellular Signaling and Expression of Adhesion Molecule by R1antTNF—Activation of TNFR1 by TNF leads to the recruitment of the adaptor protein TRADD to its cytoplasmic death domain and induction of apoptosis because of the activation of caspase-8/10 and caspase-3/7 (34). If R1antTNF inhibited the wtTNF-mediated cytotoxicity

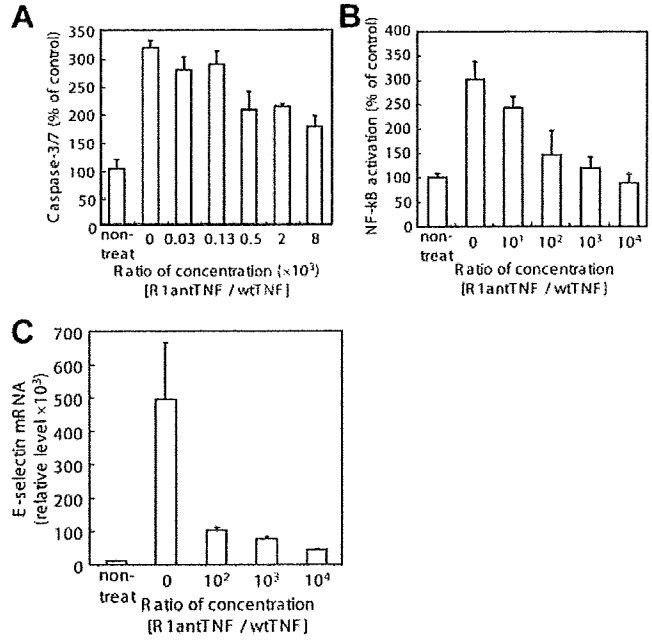

FIGURE 3. **R1antTNF-mediated inhibition of signal transduction and expression of adhesion molecule.** Activation of caspase-3/7 (*A*) and NF-κB (*B*) induced by the human wtTNF (60 and 5 ng/ml, respectively) in L-M cells was measured as described under "Experimental Procedures." Incubation times for the caspase-3/7 was 8 h and that for the NF-κB was 1 h. *C*, to measure the E-selectin expression, indicated amounts of R1antTNF were mixed with the human wtTNF (10 ng/ml), and the mixture was added to the HUVEC and incubated for 3 h. Total RNAs were prepared from these cells and were used for the RT-PCR analysis. Each data point represents the mean ± S.D.

in L-M cells by blocking the binding of wtTNF to TNFR1, R1antTNF could also inhibit this activation of caspase cascade. Thus, we investigated the inhibitory activity of R1antTNF on the wtTNF-induced activation of caspase-3/7. Indeed R1antTNF significantly inhibited the caspase-3/7 activation induced by the wtTNF in L-M cells in a dose-dependent manner (Fig. 3*A*). TNFR1 signaling also activates the transcription factor NF-κB, leading to the activation of inflammatory and anti-apoptotic genes (34). We found that the wtTNF-mediated NF-κB activation in mouse L-M cells was completely blocked by the addition of R1antTNF (Fig. 3*B*). NF-κB activated by the TNF/TNFR1 interaction regulates several cell adhesion molecules in the endothelial cells, such as E-selectin, ICAM-1, and VCAM-1 (35). Therefore, we assessed the inhibitory activity of R1antTNF on the wtTNF-induced expression of cell adhesion molecules in HUVEC cells. We found that the R1antTNF suppressed the expression of the E-selectin gene (Fig. 3*C*). These results suggested that R1antTNF inhibited the function of wtTNF by blocking the wtTNF-induced signal transduction.

TNFR1-selective Antagonistic Activity of R1antTNF—To determine the potency of the TNFR1-selective antagonistic activity, we used competitive ELISA to investigate whether the R1antTNF would inhibit only the binding of the wtTNF to hTNFR1. R1antTNF inhibited the binding of wtTNF to hTNFR1 in a dose-dependent manner just like the wtTNF did, but it did not affect the binding of wtTNF to hTNFR2 (Fig. 4, *A* and *B*). This result correlates to the results obtained using the BIAcore technique. To confirm that this antagonistic activity of R1antTNF was receptor-selective, a competitive bioassay was

Downloaded from www.jbc.org at OSAKA UNIVERSITY on March 13, 2008

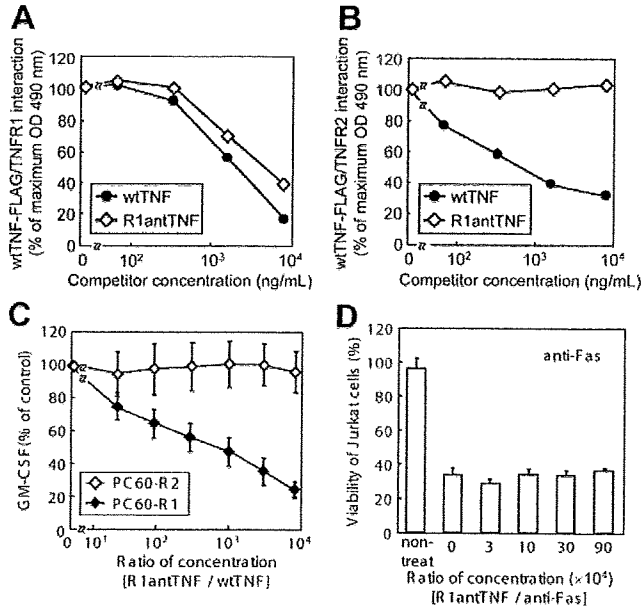

FIGURE 4. **TNFR1-selective antagonistic properties of R1antTNF.** Different concentrations of wtTNF and R1antTNF were premixed with a fixed concentration of wtTNF-FLAG and were added to the hTNFR1-coated (*A*) or hTNFR2-coated plates (*B*). Binding of wtTNF-FLAG was determined as described under "Experimental Procedures." *C*, to determine the receptor-type contribution to bioactivity, serially diluted R1antTNF was mixed with the human wtTNF (PC60-R1, 200 ng/ml; PC60-R2, 40 ng/ml), and added to the PC60-Rs cells. After 24 h, production of the rat GM-CSF was measured by ELISA as described under "Experimental Procedures." ♦, PC60-R1; 224, PC60-R2. *D*, Jurkat cells were incubated with the anti-human Fas IgM (0.2 ng/ml) and indicated dilutions of R1antTNF for 24 h, and cytotoxicity was assessed using the 3-(4,5-dimethylthiazol-2-yl)-2,5-diphenyltetrazolium bromide assay.

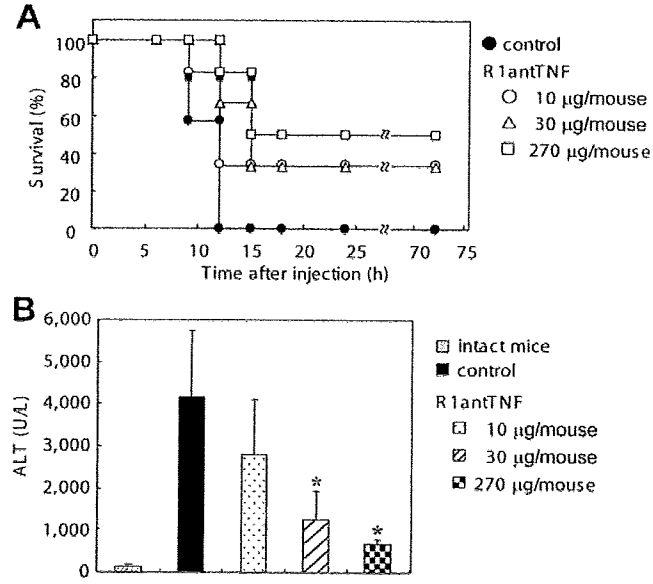

FIGURE 5. **Therapeutic effect of R1antTNF in lethal hepatitis model.** Mice were injected intravenously with recombinant human TNF (1.0 μg)/GalN (20 mg) and R1antTNF or PBS. *A*, survival rates of the mice in the TNF/GalN-induced hepatitis model were measured over a period of 72 h ($n = 6$). *B*, blood samples were collected 9 h after the challenge. Serum concentration of alanine aminotransferase (*ALT*) was measured as described under "Experimental Procedures" ($n = 6$). Data represent the mean ± S.E. Statistical significance *versus* control mice was calculated by unpaired Student's *t* test (*, $p < 0.05$).

TABLE 3
Binding properties of R1antTNF

Receptor	Kinetic parameter	wtTNF	R1antTNF
hTNFR1	k_{on} ($\times 10^5$ $M^{-1}s^{-1}$)[a]	3.6 ± 2.9	8.3 ± 0.1
	k_{off} ($\times 10^{-4}$ s^{-1})[b]	5.0 ± 1.3	28.7 ± 5.9
	K_D ($\times 10^{-9}$ M)[c]	1.4 ± 2.7	3.5 ± 1.8
hTNFR2	k_{on} ($\times 10^5$ $M^{-1}s^{-1}$)	7.0 ± 3.2	0.000001 ± 0.0
	k_{off} ($\times 10^{-4}$ s^{-1})	14.5 ± 4.9	0.1 ± 0.0
	K_D ($\times 10^{-9}$ M)	2.1 ± 1.1	92,900 ± 96.1
mTNFR1	k_{on} ($\times 10^5$ $M^{-1}s^{-1}$)	2.5 ± 0.0	18.7 ± 0.2
	k_{off} ($\times 10^{-4}$ s^{-1})	1.9 ± 0.3	96.6 ± 0.8
	K_D ($\times 10^{-9}$ M)	0.8 ± 0.4	5.2 ± 0.5

[a] k_{on} is the association kinetic constant.
[b] k_{off} is the dissociation kinetic constant.
[c] K_D is the equilibrium dissociation constant. Kinetic parameters for each TNF was calculated from the respective sensorgram by BIAevaluation 3.0 software.

performed using PC60-R1 and PC60-R2 cell lines that stably expressed hTNFR1 and hTNFR2 (25), respectively. R1antTNF efficiently inhibited the wtTNF-induced GM-CSF production in the PC60-R1 cells but not in the PC60-R2 cells (Fig. 4*C*), confirming the TNFR1-specific antagonistic activity. The risk of cross-activity to other TNF receptor superfamily members was assessed by Fas-induced cytotoxicity assay on Jurkat cell (Fig. 4*D*). R1antTNF did not affect the Fas-mediated signaling, which suggest that R1antTNF was highly selective proteo-antagonist of TNFR1. These data suggest that the R1antTNF not only binds to the TNFR1 selectively but also has TNFR1-selective inhibitory activity.

Therapeutic Efficacy of R1antTNF on Lethal Hepatitis Model—To assess the inhibitory activity and therapeutic effect of R1antTNF *in vivo*, we investigated the protective effect of R1antTNF in the TNF/D-(+)-galactosamine (GalN)-induced hepatitis model. GalN is a hepatotoxin that inhibits transcription and translation in hepatocytes. The combined administration of GalN and TNF causes massive apoptosis of hepatocytes and induces lethal hepatitis (36). In the control group, all mice died within 12 h after a lethal challenge with TNF/GalN (Fig. 5*A*). Co-treatment with R1antTNF improved the survival rate. Especially, in mice co-treated with R1antTNF (270 μg/mouse), the survival rates were 5/6 after 12 h and 3/6 after 24 h (Fig. 5*A*). The surviving mice were still alive several weeks after the treatment. In the control group, the serum levels of ALT, a marker for liver damage, were markedly elevated. In contrast, co-treatment of mice with R1antTNF suppressed the elevation of ALT levels in a dose-dependent manner (Fig. 5*B*). These results demonstrated that R1antTNF had antagonistic activity not only *in vitro* but also *in vivo*, and exhibited remarkable inhibitory effect on hepatitis.

Binding Mode and Affinity of R1antTNF—The dissociation constant (K_d) of R1antTNF binding to hTNFR1 was very similar to that of the wtTNF (Table 2), whereas the R1antTNF (mutTNF-T2) has no bioactivity through TNFR1 (Fig. 2*A*). We predicted that the binding modes of the wtTNF and R1antTNF to the TNFR1 are different, resulting in different biological activities. To quantify the altered binding mode of R1antTNF, we examined the binding kinetics of the R1antTNF for the mTNFR1, hTNFR1, and hTNFR2 using the surface plasmon resonance technique (Table 3). Indeed, the dissociation kinetic constants (k_{off}) of the R1antTNF for the human and mouse

Downloaded from www.jbc.org at OSAKA UNIVERSITY on March 1?, 08

TNFR1 (hTNFR1, $16.0 \times 10^{-4}\,s^{-1}$; mTNFR1, $37.0 \times 10^{-4}\,s^{-1}$) were clearly higher than those of the wtTNF (hTNFR1, $3.0 \times 10^{-4}\,s^{-1}$; mTNFR1, $1.5 \times 10^{-4}\,s^{-1}$). The association kinetic constants (k_{on}) of the R1antTNF for the human and mouse TNFR1 were also higher than those of the wtTNF. These results suggest that the R1antTNF interacts with the TNFR1 by repeating very quick binding and dissociation, and has a binding mode that is different from that of the wtTNF.

TABLE 4

X-ray data collection and refinement statistics (molecular replacement)

Crystal	R1antTNF
Data collection	
Space group	$P2_12_12_1$
Cell dimensions	
a, *b*, *c* (Å)	66.56, 66.97, 103.56
Resolution (Å)	50.0-1.80 (1.86-1.80)[a]
R_{merge}	0.063 (0.484)
$I/\sigma I$	36.8 (2.71)
Completeness (%)	99.6 (96.1)
Redundancy	7.1 (6.0)
Refinement	
Resolution (Å)	41.0-1.80
No. of reflections	42,155
R_{work}/R_{free}	19.8/23.9
No. of atoms	
Protein	3384
Water	237
Root mean squares deviations	
Bond lengths (Å)	0.00840
Bond angles (°)	1.47

[a] Highest resolution shell is shown in parentheses.

Crystal Structure of R1antTNF—To understand the structural basis for the different binding mode and absence of signal transduction via the R1antTNF, we examined the structure of R1antTNF by x-ray crystallography. After establishing crystallization conditions, good quality crystals of R1antTNF were obtained. The R1antTNF crystal size was $\sim 0.2 \times 0.2 \times 0.4\ mm^3$. X-ray diffraction data were collected in SPring-8 (the large synchrotron radiation facility in Japan). Analysis of these data show that the space group is $P2_12_12_1$, and the lattice constants are $a = 64.56$, $b = 66.97$, and $c = 103.56$ Å (Table 4). The R1antTNF structure was further refined using CNS. Results of the model validation using the Procheck were as follows: 88.4% residues in the most favored regions; 11.0% residues in the additional allowed regions; 0.6% residues in the generously allowed regions; and 0.0% residues in the disallowed regions. The overall structure of the R1antTNF was a trimer (Fig. 6*A*) (PDB code 2E7A), which was similar to that of the wtTNF trimer (Fig. 6*B*) (PDB code 1TNF) (37). Interestingly, structural superposition of the R1antTNF and human wtTNF showed extraordinary similarity (root mean square deviation 1.17 Å for 444 C-α atoms) of their overall structures despite their contradictory functions (Fig. 6*C*). It is believed that the TNF signaling is initiated by the formation of a complex with the three TNFRs on the cell surface. However, the fact that the R1antTNF did not transduce signaling suggests that there might be other structural differences between the wtTNF and R1antTNF.

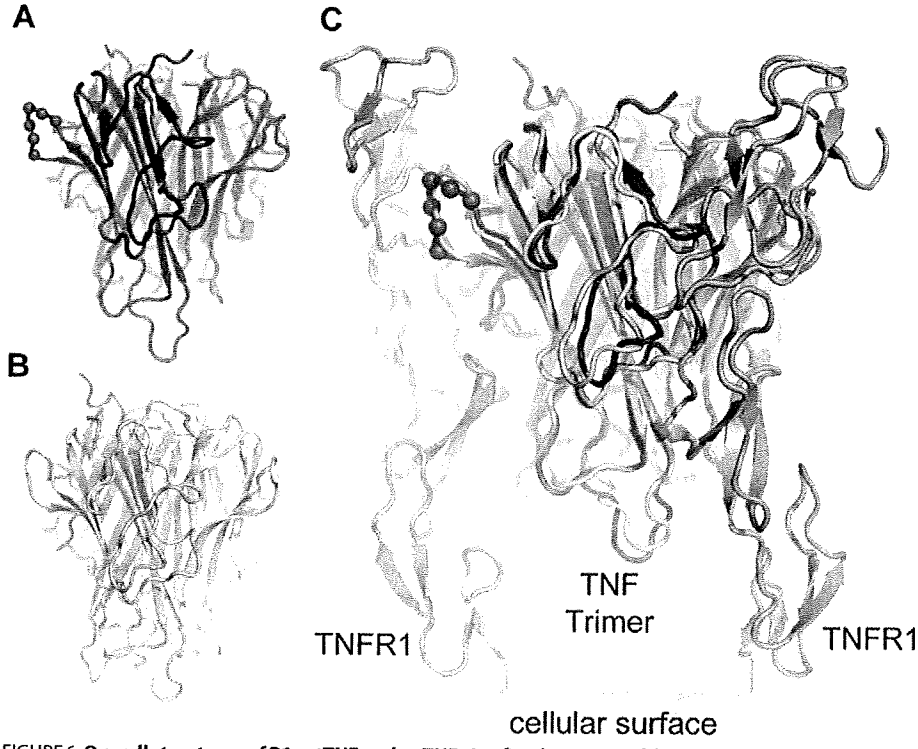

FIGURE 6. **Overall structures of R1antTNF and wtTNF.** *A*, refined structure of the R1antTNF trimer (*green*). *Blue spheres* show the mutated residues(amino acids 84–89) in R1antTNF. This structure is registered in the PDB (PDB code 2E7A). *B*, structure of the wtTNF trimer (*gray*). This structure has been published, and its PDB code is 1TNF. *C*, model structures of the TNF-TNFR1 complexes. Each TNF is superposed on the LT-α derived from the LT-α-TNFR1 complex (PDB code 1TNR). TNF binds to three R1 monomers on the cell surface. TNFR1s are shown using *red schematics*. Superposition of the structures of the wtTNF and R1antTNF was performed using the ccp4i program.

DISCUSSION

TNF, secreted from the site of injury or because of the activation of the immune cells, is involved in the development of inflammatory diseases, and it predominantly activates TNFR1 (40, 41). The TNFR1 knock-out mice have been reported to be resistant to the onset of several inflammatory diseases, such as sepsis, rheumatoid arthritis, and multiple sclerosis (14, 16, 42). In agreement with this, blocking the interaction between the TNF and TNFR1 has emerged as a powerful and clinically effective therapy for the acute inflammation and autoimmune conditions. In this study, we generated TNFR1-selective antagonistic TNF mutants using a phage library displaying structural variants of human TNF.

Among 10 potential candidates, the mutTNF-T2 (R1antTNF) selectively and strongly bound to the TNFR1 but showed almost no bioactivity. Additionally, we found that R1antTNF most effectively inhibited the wtTNF-induced cell death

Downloaded from www.jbc.org at OSAKA UNIVERSITY on March 13, 2008

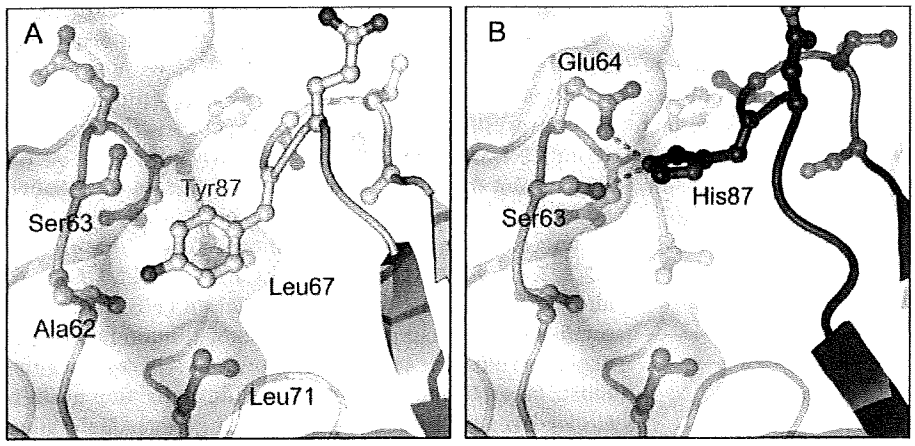

FIGURE 7. **Structural difference between the receptor binding region of the R1antTNF and wtTNF.** *A,* interaction between the wtTNF (*gray*) and TNFR1 (*red*). *White layer* depicts the molecular surface of the TNFR1. Hydrophobic interaction is formed between the Tyr-87 and molecular pocket in the TNFR1 (Leu-67, Leu-71, Ala-62, and Ser-63). *B,* interaction between the R1antTNF (*green*) and TNFR1 (*red*). *Yellow broken lines* show the possible interactions of the R1antTNF His-87 with the receptor Ser-63 and Glu-64. In this simulation, the side chains of each structure were rotated to fit the predicted interaction. Stable structures of these rotamers were constructed using the O program.

(Fig. 3*B*). R1antTNF also clearly inhibited the TNF functions other than cytotoxicity. Interestingly, the ratio between the R1antTNF and wtTNF was 1000-fold or more to obtain 50% inhibition against the wtTNF-induced cytotoxicity and caspase-3/7 activity, whereas the ratio was only about 100-fold or less to obtain 50% inhibition against the wtTNF-induced expression of E-selectin, production of GM-CSF, and NF-κB activation. Intracellular signaling induced by the TNF/TNFR1 interaction is divided into the following two main pathways: (i) the NF-κB pathway, which regulates the expression of adhesion molecules and inflammatory cytokines, and (ii) the caspase cascade, which induces cell death through apoptosis or necrosis (34). Our results suggest that R1antTNF is more antagonistic against the wtTNF function mediated via the NF-κB pathway than via the caspase cascade. In pathological tissues, endogenous TNF induced expression of the cell adhesion molecules and inflammatory cytokines resulting in leukocyte infiltration, which are regulated by NF-κB and are closely related to the development or exacerbation of diseases (43) such as fulminant hepatitis and rheumatoid arthritis. Because the R1antTNF efficiently inhibited the TNF-induced NF-κB activation, it would be of therapeutic value for the treatment of such inflammatory diseases. These cell line or signaling pathway-dependent differences in the inhibitory efficiencies of R1antTNF could be valuable in studying the structural or biological changes caused by the TNF/TNFR1 interactions, which need to be explored further.

We examined the therapeutic effects of R1antTNF in the acute lethal hepatitis model. R1antTNF exhibited the suppressive effect on acute hepatitis. Although the R1antTNF suppressed the elevation of the ALT level in a dose-dependent manner, the survival rate was not significantly improved between the dose 10 μg/mouse *versus* 270 μg/mouse. This discrepancy is likely because the difference in the degree of suppression of the elevated ALT level does not always correlate well with the improvement in the survival rate. Nevertheless, treatment with only 30–270 μg/mouse R1antTNF (30–270-fold excess over wtTNF) significantly suppressed the elevation of ALT levels and reduced the lethal toxicity. Thus, the antagonistic activity of R1antTNF *in vivo* was stronger than expected from the *in vitro* results. The TNF/GalN-mediated activation of TNFR1 not only induces apoptosis and necrosis of hepatocytes but also induces inflammatory responses and secondary responses associated with the cell death (44). Therefore, we believe that the R1antTNF exerted its therapeutic effect by comprehensively inhibiting the TNF/GalN-mediated biological responses, thus blocking the liver failure in the experimental animals. The R1antTNF is also expected to have therapeutic effect in chronic inflammatory disease models, such as in collagen-induced arthritis model and experimental autoimmune encephalomyelitis model. However, the plasma half-life of R1antTNF, like the wtTNF, is very short (12 min). We recently developed a novel PEGylation system that dramatically improved the *in vivo* stability and therapeutic effects of the bioactive proteins (29, 45). We are currently in the process of developing the PEGylated R1antTNF to further enhance its potential anti-inflammatory activity.

To explore the underlying mechanism of the antagonistic activity of R1antTNF, we examined the crystal structure of R1antTNF by x-ray crystallography. Despite close resemblance between the crystal structure of the R1antTNF and wtTNF, the receptor-bound R1antTNF did not transmit any signal via the TNFR1. To further speculate why the R1antTNF showed antagonistic activity, we utilized the superpose program to perform docking simulations with the TNFs and TNFR1 using the crystal structure of the LT-α-TNFR1 complex (PDB code 1TNR) (31). The TNF-TNFR1 model complex suggested that the Tyr-87 of the wtTNF, an essential residue, is buried in a molecular hydrophobic "pocket" of the TNFR1, which houses the receptor residues Leu-67 and Leu-71 that are implicated to maintain the TNF and TNFR1 complex (Fig. 7*A*). Tyr-87 is a highly conserved residue throughout the TNF superfamily, such as LT-α, LT-β and LIGHT, and this discussion is also reflected in the crystal structure of the LT-α-TNFR1 complex (38). Accordingly, site-directed mutagenesis of the Tyr-87 residue of TNF resulted in a dramatic loss of its biological activity and affinities for both TNFRs (39), suggesting that this residue is be essential for TNF function. However, in R1antTNF, the Tyr-87 is replaced with a histidine residue. The structural simulation studies suggested that the His-87 in R1antTNF could interact with the relatively negatively charged Ser-63 and Glu-64 residues on the TNFR1 surface, which probably explains the different binding mode of the R1antTNF as compared with the wtTNF (Fig. 7*B*).

Downloaded from www.jbc.org at OSAKA UNIVERSITY on March 1?, 08

Indeed, the association and dissociation kinetic constants (k_{on} and k_{off}, respectively) for the binding of R1antTNF to TNFR1 were considerably higher than those of the wtTNF, indicating a difference in the TNFR1-binding pattern between the wtTNF and R1antTNF (Table 3). The association and dissociation kinetic constants are very important factors in discussing the ligand-receptor interaction and function. It was previously shown that the membrane-bound TNF, but not the soluble TNF, could activate the TNFR2, and the reason for this difference was attributed to the dissociation kinetic constant of the soluble TNF, which was much higher than the membrane-bound TNF (46). Therefore, the inability of R1antTNF to transmit signal and its antagonistic activity are probably because of the higher k_{on} and k_{off} values of R1antTNF for the TNFR1, suggesting that they influenced the stability of the TNF-TNFR1 complex and reduced the continuous binding time required for the signal transmission. In addition, we demonstrated that R1antTNF inhibited the activations of both caspase-3/7 and NF-κB (Fig. 5, *A* and *B*), which are mediated via two distinct intracellular signaling complexes. TNF/TNFR1-mediated signaling requires sequential formation of the following two receptor complexes: the complex I is involved in the recruitment of TRADD, RIP1, and TRAF2 leading to the NF-κB activation, whereas the consequent complex II is involved in internalization, post-translational modifications, and recruitment of FADD and caspase-8 initiating apoptosis (47). Together, these results suggest that R1antTNF blocked the TNF-mediated signal transmission by binding to TNFR1 in a rapid association/dissociation cycle, thereby inhibiting the formation of the intracellular complexes. However, more detailed investigations, such as detection of these intracellular complexes and their internalization, other TNF/TNFR1-mediated signaling, and analysis of the complex structure of the R1antTNF and TNFR1, are required to elucidate exactly how the R1antTNF exhibits its TNFR1 antagonistic activity.

We succeeded in developing the first mutant form of the human TNF with TNFR1-selective antagonistic activity by using a unique combinatorial phage-based technique. Existing TNF blockers, *i.e.* etanercept and infliximab, are widely used in the treatment of rheumatoid arthritis and Crohn disease (5). But these drugs, which prevent TNF binding on both TNF receptor types, can cause serious side effects, such as mycobacterial infections and hepatitis B virus infection (48). Although TNFR1 is believed to be important for immunological responses (42), TNFR2 is thought to be also important for antiviral resistance and is effective for controlling the mycobacterial infection by affecting the membrane-bound TNF stimulation (18, 49). Therefore, this mutant TNF, R1antTNF, might be a new therapeutic drug with reduced side effects. We are currently evaluating not only the therapeutic effect of R1antTNF on rheumatoid arthritis or experimental encephalomyelitis model, and but also its side effects such as mycobacterial and virus infection. Finally, our studies demonstrate the feasibility of generating TNF receptor subtype-selective antagonistic mutants by comprehensive substitution of sets of amino acids in the wild-type ligand proteins. Our data also suggest that this combinatorial biosynthetic strategy using the bioactive protein as the "lead protein" is very effective in creating receptor-specific agonists and antagonists, and we believe that this approach will generate protein drugs of improved therapeutic value.

Acknowledgment—We thank E. C. Gabazza for discussions and critical reading of the manuscript.

REFERENCES

1. Aggarwal, B. B. (2003) *Nat. Rev. Immunol.* **3,** 745–756
2. Aderka, D., Engelmann, H., Maor, Y., Brakebusch, C., and Wallach, D. (1992) *J. Exp. Med.* **175,** 323–329
3. Feldmann, M., and Maini, R. N. (2003) *Nat. Med.* **9,** 1245–1250
4. Muto, Y., Nouri-Aria, K. T., Meager, A., Alexander, G. J., Eddleston, A. L., and Williams, R. (1988) *Lancet* **2,** 72–74
5. Feldmann, M. (2002) *Nat. Rev. Immunol.* **2,** 364–371
6. Goldbach-Mansky, R., and Lipsky, P. E. (2003) *Annu. Rev. Med.* **54,** 197–216
7. Brown, S. L., Greene, M. H., Gershon, S. K., Edwards, E. T., and Braun, M. M. (2002) *Arthritis Rheum.* **46,** 3151–3158
8. Keane, J., Gershon, S., Wise, R. P., Mirabile-Levens, E., Kasznica, J., Schwieterman, W. D., Siegel, J. N., and Braun, M. M. (2001) *N. Engl. J. Med.* **345,** 1098–1104
9. Nathan, D. M., Angus, P. W., and Gibson, P. R. (2006) *J. Gastroenterol. Hepatol.* **21,** 1366–1371
10. Shakoor, N., Michalska, M., Harris, C. A., and Block, J. A. (2002) *Lancet* **359,** 579–580
11. Sicotte, N. L., and Voskuhl, R. R. (2001) *Neurology* **57,** 1885–1888
12. Aggarwal, B. B., Eessalu, T. E., and Hass, P. E. (1985) *Nature* **318,** 665–667
13. Leist, M., Gantner, F., Jilg, S., and Wendel, A. (1995) *J. Immunol.* **154,** 1307–1316
14. Mori, L., Iselin, S., De Libero, G., and Lesslauer, W. (1996) *J. Immunol.* **157,** 3178–3182
15. Liu, J., Marino, M. W., Wong, G., Grail, D., Dunn, A., Bettadapura, J., Slavin, A. J., Old, L., and Bernard, C. C. (1998) *Nat. Med.* **4,** 78–83
16. Kassiotis, G., and Kollias, G. (2001) *J. Exp. Med.* **193,** 427–434
17. Fremond, C., Allie, N., Dambuza, I., Grivennikov, S. I., Yeremeev, V., Quesniaux, V. F., Jacobs, M., and Ryffel, B. (2005) *Respir. Res.* **6,** 136
18. Olleros, M. L., Guler, R., Corazza, N., Vesin, D., Eugster, H. P., Marchal, G., Chavarot, P., Mueller, C., and Garcia, I. (2002) *J. Immunol.* **168,** 3394–3401
19. Grell, M., Becke, F. M., Wajant, H., Mannel, D. N., and Scheurich, P. (1998) *Eur. J. Immunol.* **28,** 257–263
20. Kafrouni, M. I., Brown, G. R., and Thiele, D. L. (2003) *J. Leukocyte Biol.* **74,** 564–571
21. Kim, E. Y., Priatel, J. J., Teh, S. J., and Teh, H. S. (2006) *J. Immunol.* **176,** 1026–1035
22. Engelmann, H., Holtmann, H., Brakebusch, C., Avni, Y. S., Sarov, I., Nophar, Y., Hadas, E., Leitner, O., and Wallach, D. (1990) *J. Biol. Chem.* **265,** 14497–14504
23. Carter, P. H., Scherle, P. A., Muckelbauer, J. K., Voss, M. E., Liu, R. Q., Thompson, L. A., Tebben, A. J., Solomon, K. A., Lo, Y. C., Li, Z., Strzemienski, P., Yang, G., Falahatpisheh, N., Xu, M., Wu, Z., Farrow, N. A., Ramnarayan, K., Wang, J., Rideout, D., Yalamoori, V., Domaille, P., Underwood, D. J., Trzaskos, J. M., Friedman, S. M., Newton, R. C., and Decicco, C. P. (2001) *Proc. Natl. Acad. Sci. U. S. A.* **98,** 11879–11884
24. Murali, R., Cheng, X., Berezov, A., Du, X., Schon, A., Freire, E., Xu, X., Chen, Y. H., and Greene, M. I. (2005) *Proc. Natl. Acad. Sci. U. S. A.* **102,** 10970–10975
25. Vandenabeele, P., Declercq, W., Vercammen, D., Van de Craen, M., Grooten, J., Loetscher, H., Brockhaus, M., Lesslauer, W., and Fiers, W. (1992) *J. Exp. Med.* **176,** 1015–1024
26. Tsutsumi, Y., Kihira, T., Tsunoda, S., Kanamori, T., Nakagawa, S., and Mayumi, T. (1995) *Br. J. Cancer* **71,** 963–968
27. Barbara, J. A., Smith, W. B., Gamble, J. R., Van Ostade, X., Vandenabeele,

Downloaded from www.jbc.org at OSAKA UNIVERSITY on March 13, 2008

P., Tavernier, J., Fiers, W., Vadas, M. A., and Lopez, A. F. (1994) *EMBO J.* **13,** 843–850
28. Brunetti, C. R., Paulose-Murphy, M., Singh, R., Qin, J., Barrett, J. W., Tardivel, A., Schneider, P., Essani, K., and McFadden, G. (2003) *Proc. Natl. Acad. Sci. U. S. A.* **100,** 4831–4836
29. Yamamoto, Y., Tsutsumi, Y., Yoshioka, Y., Nishibata, T., Kobayashi, K., Okamoto, T., Mukai, Y., Shimizu, T., Nakagawa, S., Nagata, S., and Mayumi, T. (2003) *Nat. Biotechnol.* **21,** 546–552
30. Potterton, E., Briggs, P., Turkenburg, M., and Dodson, E. (2003) *Acta Crystallogr. Sect. D. Biol. Crystallogr.* **59,** 1131–1137
31. Banner, D. W., D'Arcy, A., Janes, W., Gentz, R., Schoenfeld, H. J., Broger, C., Loetscher, H., and Lesslauer, W. (1993) *Cell* **73,** 431–445
32. Jones, T. A., Zou, J. Y., Cowan, S. W., and Kjeldgaard, M. (1991) *Acta Crystallogr. Sect. A.* **47,** 110–119
33. Brunger, A. T., Adams, P. D., Clore, G. M., DeLano, W. L., Gros, P., Grosse-Kunstleve, R. W., Jiang, J. S., Kuszewski, J., Nilges, M., Pannu, N. S., Read, R. J., Rice, L. M., Simonson, T., and Warren, G. L. (1998) *Acta Crystallogr. Sect. D. Biol. Crystallogr.* **54,** 905–921
34. Chen, G., and Goeddel, D. V. (2002) *Science* **296,** 1634–1635
35. Mackay, F., Loetscher, H., Stueber, D., Gehr, G., and Lesslauer, W. (1993) *J. Exp. Med.* **177,** 1277–1286
36. Hishinuma, I., Nagakawa, J., Hirota, K., Miyamoto, K., Tsukidate, K., Yamanaka, T., Katayama, K., and Yamatsu, I. (1990) *Hepatology* **12,** 1187–1191
37. Eck, M. J., and Sprang, S. R. (1989) *J. Biol. Chem.* **264,** 17595–17605
38. Harrop, J. A., McDonnell, P. C., Brigham-Burke, M., Lyn, S. D., Minton, J., Tan, K. B., Dede, K., Spampanato, J., Silverman, C., Hensley, P., DiPrinzio, R., Emery, J. G., Deen, K., Eichman, C., Chabot-Fletcher, M., Truneh, A., and Young, P. R. (1998) *J. Biol. Chem.* **273,** 27548–27556
39. Zhang, X. M., Weber, I., and Chen, M. J. (1992) *J. Biol. Chem.* **267,** 24069–24075
40. Ruuls, S. R., Hoek, R. M., Ngo, V. N., McNeil, T., Lucian, L. A., Janatpour, M. J., Korner, H., Scheerens, H., Hessel, E. M., Cyster, J. G., McEvoy, L. M., and Sedgwick, J. D. (2001) *Immunity* **15,** 533–543
41. Grell, M., Douni, E., Wajant, H., Lohden, M., Clauss, M., Maxeiner, B., Georgopoulos, S., Lesslauer, W., Kollias, G., Pfizenmaier, K., and Scheurich, P. (1995) *Cell* **83,** 793–802
42. Rothe, J., Lesslauer, W., Lotscher, H., Lang, Y., Koebel, P., Kontgen, F., Althage, A., Zinkernagel, R., Steinmetz, M., and Bluethmann, H. (1993) *Nature* **364,** 798–802
43. Zhou, A., Scoggin, S., Gaynor, R. B., and Williams, N. S. (2003) *Oncogene* **22,** 2054–2064
44. Nagaki, M., Sugiyama, A., Osawa, Y., Naiki, T., Nakashima, S., Nozawa, Y., and Moriwaki, H. (1999) *J. Hepatol.* **31,** 997–1005
45. Kamada, H., Tsutsumi, Y., Sato-Kamada, K., Yamamoto, Y., Yoshioka, Y., Okamoto, T., Nakagawa, S., Nagata, S., and Mayumi, T. (2003) *Nat. Biotechnol.* **21,** 399–404
46. Krippner-Heidenreich, A., Tubing, F., Bryde, S., Willi, S., Zimmermann, G., and Scheurich, P. (2002) *J. Biol. Chem.* **277,** 44155–44163
47. Micheau, O., and Tschopp, J. (2003) *Cell* **114,** 181–190
48. Gomez-Reino, J. J., Carmona, L., Valverde, V. R., Mola, E. M., and Montero, M. D. (2003) *Arthritis Rheum.* **48,** 2122–2127
49. Saunders, B. M., Tran, S., Ruuls, S., Sedgwick, J. D., Briscoe, H., and Britton, W. J. (2005) *J. Immunol.* **174,** 4852–4859

Downloaded from www.jbc.org at OSAKA UNIVERSITY on March 1[illegible]08

Laboratory of Pharmaceutical Proteomics[1], National Institute of Biomedical Innovation (NIBIO), Graduate School of Pharmaceutical Sciences[2], Center of Advanced Medical Engineering and Informatics[3], Osaka University, Osaka, Japan

Effect of protein properties on display efficiency using the M13 phage display system

S. Imai[1, 2], Y. Mukai[1, 2], T. Takeda[1], Y. Abe[1], K. Nagano[1, 2], H. Kamada[1, 3], S. Nakagawa[2], S. Tsunoda[1, 3], Y. Tsutsumi[1, 2, 3]

Received May 15, 2008, accepted May 21, 2008

Shin-ichi Tsunoda, Ph.D., Laboratory of Pharmaceutical Proteomics, National Institute of Biomedical Innovation (NIBIO), 7-6-8 Saito-Asagi, Ibaraki, Osaka 567-0085, Japan
tsunoda@nibio.go.jp

Pharmazie 63: 760–764 (2008) *doi: 10.1691/ph.2008.8132*

The M13 phage display system is a powerful technology for engineering proteins such as functional mutant proteins and peptides. In this system, it is necessary that the protein is displayed on the phage surface. Therefore, its application is often limited when a protein is poorly displayed. In this study, we attempted to understand the relationship between a protein's properties and its display efficiency using the well-known pIII and pVIII type phage display system. The display of positively charged SV40 NLS and HIV-1 Tat peptides on pIII was less efficient than that of the neutrally charged RGDS peptide. When different molecular weight proteins (1.5–58 kDa) were displayed on pIII and pVIII, their display efficiencies were directly influenced by their molecular weights. These results indicate the usefulness in predicting a desired protein's compatibility with protein and peptide engineering using the phage display system.

1. Introduction

Phage display systems have attracted much attention as the best technology to create functional mutant proteins and peptides ever since Smith et al. reported that random peptides could be displayed on the surface of filamentous M13 phage (Smith 1985). Many researchers have applied this system in attempts to create human antibodies and tissue-specific peptides (Schier et al. 1996; Maruta et al. 2003; Imai et al. 2006). Indeed, we have been successful in creating a useful mutant TNF to be used as a drug (Shibata et al. 2004; Yamamoto et al. 2003). Thus, the phage display system has a wide range of applications (Stich et al. 2003; Gourdine et al. 2005; Takashima et al. 2000).

Filamentous M13 phage has a circular single stranded DNA and takes the form of a long tube that consists of eleven kinds of proteins. This virus effectively proliferates upon infection of *E. coli* (Sidhu 2001; Bayer and Feigenson 1985; Kuhn 1987). In the phage display system, a fusion protein composed of target-molecule and coat protein is derived from a phagemid vector, and wild-type phage composition proteins (pI–pXI) are derived from a helper phage genome. These components can make phage libraries that display target-molecules by assembling within the periplasm of *E. coli*. The most useful characteristic of this system is that protein libraries can be displayed easily on the phage surface by inserting gene libraries within the phage genome. Target-molecules are obtained rapidly by the use of an *in vitro* affinity panning procedure that selects and amplifies specific phage clones (Smith 1985).

In the phage display system, target-molecules can be displayed on coat proteins (pIII, pVI, pVII, pVIII, pIX), though generally they are displayed on pIII or pVIII. Displaying 0–1 molecule per phage in the pIII type phage display system is suitable for isolating high-affinity molecules (Chasteen et al. 2006; Keresztessy et al. 2006). Alternatively, ten molecules can be displayed on a phage particle in the pVIII type phage display system to select low-affinity molecules (Verhaert et al. 1999; Kneissel et al. 1999; Lowman 1997).

As described, the phage display system is the most useful tool to create bioactive peptides and functional mutant proteins. However, because the efficiency of display is influenced by the properties of the target protein (molecular weight, electric charge, etc.), poor display often limits its application. Despite this problem, there is little research examining the relationship between display efficiency and a protein's properties. Thus, studies are warranted in order to apply the phage display system effectively. In this report, we prepared phages that displayed proteins of different molecular weights and electric charges to ascertain the relationship between display efficiency and protein properties.

2. Investigations, results and discussion

In this study we examined the relationship between protein properties (molecular weight, electric charge etc.) and the efficiency of display with pIII and pVIII coat proteins of the filamentous M13 phage display system (Fig. 1). To begin with, we prepared phages that displayed different electrically charged peptides on pIII (Fig. 2B) and evalu-

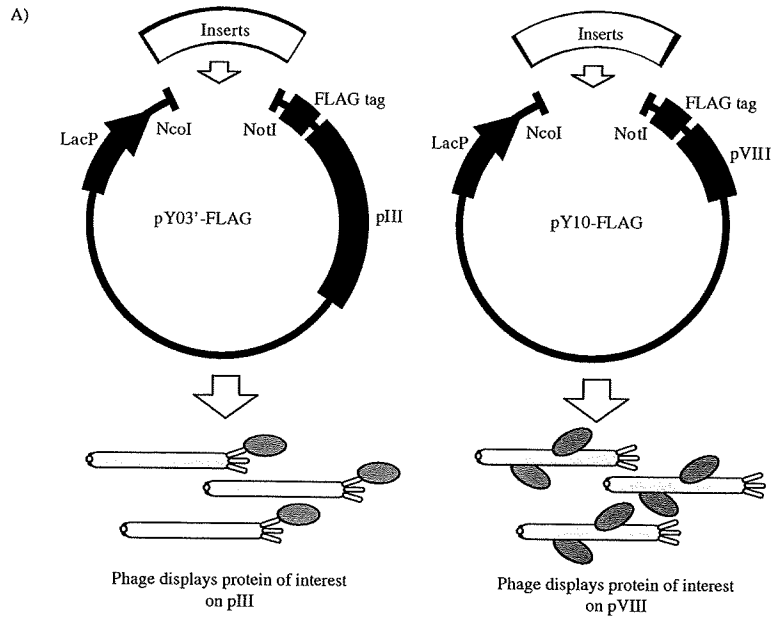

B)

Inserts	Molecular weight (Da)	pI
RGDS peptide (RGDS)	443	6.4
SV40 NLS peptide (PKKKRKV)	883	11.9
HIV-Tat peptide (YGRKKRRQRRR)	1,559	12.8
LacZ-α	11,000	5.2
anti-KDR scFv	25,000	5.0
Importin-α	58,000	5.1

Fig. 1:
Construction of phagemid vectors encoding different proteins or peptides.
A) Different inserts were cloned into pY03′-FLAG and pY10-FLAG phagemid vectors. Phage particles displaying proteins fused to pIII and pVIII were prepared from pY03′-FLAG and pY10-FLAG, respectively. B) Different inserts and their molecular weights

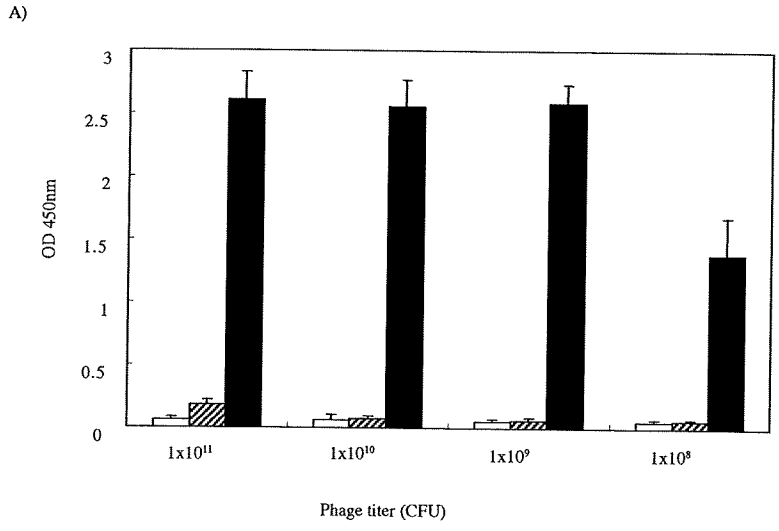

B)

	sequence	M.W. (Da)	pI
□ Tat peptide	YGRKKRRQRRR	1,559	12.8
▨ SV40 NLS	PKKKRKV	883	11.9
■ RGDS peptide	RGDS	433	6.4

Fig. 2:
Influence of the efficiency of peptide-display by the ionic charge of peptides.
The efficiency of peptide-display on pIII was assessed by phage ELISA. Displayed peptides were fused to FLAG-tag – pIII on the phage particle and captured by immobilized anti-FLAG antibody. After washing, the number of captured phage was assessed by anti-M13 HRP conjugate. Two positively charged peptides (Tat peptide; □ and SV40 NLS; ▨) and a neutral peptide (RGDS; ■) were used in this experiment (n = 3). Each data value represents the mean ± S.D. B) Sequences of displayed peptides and their pIs. Cationic amino acids are underlined. All pI values were calculated by Expasy Compute pI/Mw tool (http://au.expasy.org)